Hindawi
Advances in Materials Science and Engineering
Volume 2021, Article ID 8701180, 11 pages
https://doi.org/10.1155/2021/8701180

Research Article

Experimental Study on the Deformation and Failure Characteristics of Anchor under Graded Loading and Corrosion

Guanglin Sun[1] **Jiangchun Hu**[1] **Hongfang Wang,**[2] **and Pengfei Li**[1,3]

[1]*School of Architecture and Civil Engineering, Zhongyuan University of Technology, Zhengzhou 450007, China*
[2]*School of Materials and Chemical Engineering, Zhongyuan University of Technology, Zhengzhou 450007, China*
[3]*China South City Co. LTD, Shenzhen 518111, China*

Correspondence should be addressed to Jiangchun Hu; hujiangchun@126.com

Received 16 May 2021; Revised 7 July 2021; Accepted 23 July 2021; Published 3 August 2021

Academic Editor: Fernando Lusquiños

During the entire life cycle of rock and soil anchors, owing to the influence of adverse factors such as the working environment, load change, and anchor performance degradation, the working load of the anchor will continue to increase and the mechanical properties will continue to deteriorate, which significantly affects the safety and stability of rock and soil anchors. Therefore, this study focuses on the deformation and failure characteristics of anchors under loading and corrosion conditions by means of indoor simulation tests under laboratory conditions. The results indicate the following. (1) There are obvious cracks on the surfaces of specimens 2# and 10#. In the two groups of specimens, the corroded bolt surface exhibited a corrosion phenomenon. This indicates that the corrosion environment conditions cause a certain degree of damage to the anchored rock mass. (2) Under the same gradient load condition, three observable cracks were found in the 10# anchorage specimens and one observable crack was found in the 2# anchorage specimens. Therefore, it is clear that the damage degree of the anchor increases with an increase in the corrosion time. (3) Under the condition of corrosion environment, the strain in the lower part of the specimen is generally greater than that in the upper part of the specimen, and the failure of this group of specimens in the loading process is mostly splitting failure, which is basically generated along the trend of the strain nephogram, and shear failure occurs with the extension and diffusion of cracks.

1. Introduction

Geotechnical anchoring technology can improve the strength and performance of geotechnical anchoring solids, which plays an important role in mining and water conservancy engineering construction [1]. The mechanical properties and durability of the anchor cable are very important for the anchorage system [2]. Hence, geotechnical anchoring technology is widely used in roadway bolt support [3], jointed rock reinforcement [4, 5], and other underground engineering constructions. Corrosion of steel members is one of the main reasons for the deterioration of concrete structures, and the corrosion grade is often used to evaluate the bond strength between steel and concrete [6]. Moreover, loading and corrosion lead to the cracking of engineering structures [7, 8]. Corrosion not only reduces the anchorage strength, durability, and safety of structures but also is an important factor affecting the durability of anchors [9–11]. Severe corrosion leads to incompatibility between steel strands and concrete stress [12]. Ou and Nguyen [13] showed that the corrosion of reinforcements had diverse effects on the failure modes of reinforced concrete beams. Karthik et al. [14] simulated the corrosion tests of large reinforced concrete beam column joints. Wang et al. [15] studied the corrosion situation and influencing factors of in-service anchors and proved that the anchor head is more vulnerable to corrosion than the anchorage section. The shear test results obtained by Lin et al. [16, 17] proved that the grouting state, the number of bolts, and the inclination angle of bolts have a significant influence on the change in the axial force of the anchor. The shear effect of the bolt connection was related to the bolt influence coefficient.

Based on the bolt influence coefficient, a modified shear strength model of the bolt connection was established. Corrosion can reduce the durability and bearing capacity of FRP concrete [18]. Al-Sibaly and Sabhan [19] found that corrosion had a significant influence on the deflection of the beam. Corrosion affects the bond strength and deformation, as well as the axial tensile properties of the reinforcement in concrete [20, 21]. Chen et al. [22] conducted mechanical tests on corroded reinforced concrete beams and found that as the corrosion degree increased, the bond strength of reinforced concrete first increased and then decreased. Imperatore et al. [23] proved that the interaction between steel and concrete can lead to the corrosion of concrete components, which can affect the bonding performance of components, and the corrosion of concrete lap joints can cause damage to the concrete protective layer [24]. Corrosion has a significant effect on the cracks and on the bond between steel and concrete [25, 26]. Berrocal et al. [27] reported that the corrosion of steel bars affects the bond performance of fiber-reinforced concrete. Corrosion of reinforcement leads to cracking of the concrete cover and a decrease in the bond strength of the reinforced concrete [28]. Therefore, factors such as acidic corrosion environment and high stress will not only accelerate the damage progress of anchorage structures but also corrode rock anchor bars or bolts, reduce the overall engineering mechanical properties of rock mass, and even cause engineering disasters.

Digital image correlation (DIC) technology is a noncontact and nondestructive image processing technology that can measure the displacement field and strain field of a specimen surface [29, 30]. To carry out digital image processing, it is necessary to apply speckle on the surface of the sample, and the noncontact method can be used to capture the full-field deformation and strain field of the sample [31]. Wu et al. [32] analyzed the digital image failure characteristics of rock samples with voids and cracks under uniaxial compression. Tang et al. [33] revealed the strain and displacement fields of a granite beam with a three-point bending notch using the DIC method. Wang et al. [34] performed uniaxial compression tests on 3D printed rock samples and analyzed the influence of discontinuous structures on rock strength using DIC technology. Dong et al. [35] used the DIC method to analyze the fracture displacement field of rock concrete composite beams in the process of three-point bending and four-point shear tests. Mata-Falcón et al. [36] used a digital image method to measure the test process of a concrete structure. Sharafisafa et al. [37] used noncontact DIC technology to analyze the deformation of the Brazilian disc test. Tinkler-Davies and Shah [38] studied the digital image processing technology of bamboo laminates under compression. Huang et al. [39] applied a DIC method to study the global displacement field of a rock tunnel with a fault. Zhang et al. [40] used digital correlation technology to study the deformation and failure tests of Sichuan sandstone samples. Zhang et al. [41] conducted experiments on semicircular sandstone and used a DIC method to analyze the displacement field of specimens with different sizes. Stewart and Garcia [42] used DIC technology to track the asphalt crack growth. Liu et al. [43] applied DIC technology to study the deformation and failure mode of the test when studying a wood beam strengthened with carbon fiber. Cao et al. [44] conducted a digital speckle study on brittle jointed rock specimens under uniaxial compression. Liang et al. [45] studied the DIC method for aluminum alloy deformation. Zhou et al. [46] studied the DIC technology of uniaxial loading for ductile rock materials with defects.

Based on the above research results, an indoor simulation experiment of the uniaxial creep behavior of an anchored rock mass under acid corrosion conditions was designed. The rock anchorage model of the reinforced rock bolt was fabricated. The creep properties of the anchored rock mass under different corrosion conditions were studied using DIC testing technology, and the uniaxial compression deformation properties of the corroded anchored rock mass were revealed. The remainder of this paper is organized as follows. The second section introduces the test method. The third section provides the test results. Finally, the fourth section presents the conclusions of the study.

2. Materials and Methods

2.1. Specimen Preparation. In the laboratory, river sand, cement, and gypsum powder were selected (mass ratio of river sand cement gypsum powder = 10 : 7 : 3) and then evenly mixed using a mixer. After the mixture was stirred uniformly, it was poured into a mold box. The inner box surface of the mold was evenly coated with a release agent. The inner space of the mold was fabricated to be 150 mm long × 150 mm wide × 150 mm high. The anchor rod and acid solution conduit were coated with planting glue. When fabricating the specimen, the mold was placed on a shaking table to ensure specimen uniformity. The diameter of the anchor rod was 5 mm. The two ends of the anchor rod were equipped with a gasket and nut, respectively. The diameter of the acid solution catheter was 4 mm. As shown in Figure 1, the acid solution conduits were arranged perpendicular to the position of the anchor rod, which was to be corroded.

When the mixture was added to 1/4 of the mold, two bottom anchor bolts were inserted and screwed with a gasket and nut. Similarly, when the mixture was added to 2/4 of the mold, two middle anchor bolts were inserted and screwed with a gasket and nut. Finally, when the mixture was added to 3/4 of the mold, two middle anchor bolts were inserted and screwed with a gasket and nut. The acid solution pipe was inserted into the two bolts on the top of the anchor solid mixture model, and the direction was perpendicular to the bolt direction. The entire specimen preparation process was carried out on a shaking table. The demolding and curing treatments were carried out 24 h after the specimen was made, and then the demolded specimen was placed in a constant-temperature curing box at 70°C for 48 h. The fabrication process of the specimens is shown in Figure 2.

After specimen curing, a layer of white pigment was smeared on the smooth surface of the specimen, and the speckle pattern was arranged on the surface. As shown in Figure 3, the corrosion of the anchor rod was realized by an acid solution conduit, and the concentration of the

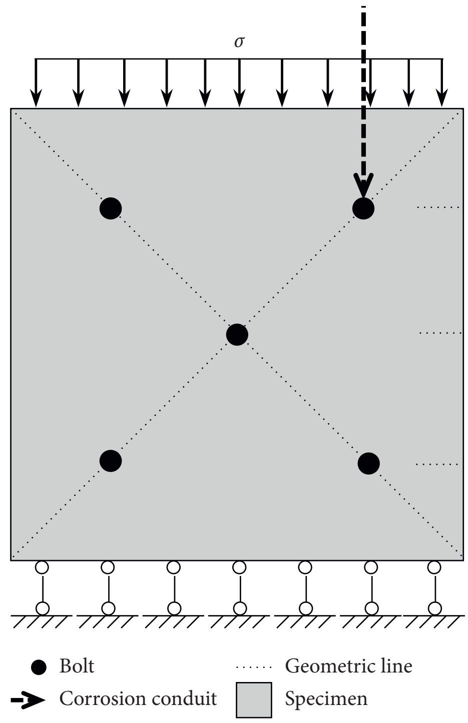

Figure 1: Specimen scheme.

corrosion solution was 50%. The corrosion times of specimens 2# and 10# were 3 and 14 d, respectively. The detailed parameters of specimens 2# and 10# are listed in Table 1.

2.2. Test Equipment. The universal pressure testing machine at Zhongyuan University of Technology (Figure 4) was used in this test. The experimental system generated an axial graded compression load on the tested specimens.

Before the loading test, the specimens were processed using a speckle pattern. High-speed cameras were used to collect deformation images of the specimens during the test (Figure 5(a)). Figure 5(b) shows the specimen loading process. In Figure 5(c), two LED lamps were arranged on both sides of the sample to negate the influence of light on the imaging environment.

3. Results and Discussion

3.1. Test Process Description. In this test, a universal press was used, and an incremental loading method was applied. The highest creep load corresponding to the sample was 80% of the corresponding load of the uniaxial compressive strength of the sample, and the loads in the other stages were 16%, 32%, 48%, and 64% of the uniaxial compressive strength, respectively. The loading time of each stage was 4 h, and the total loading time was approximately 20 h. The loading path and overall deformation of the specimen during the test are plotted in Figure 6.

The overall deformation curve of sample 2#, shown in Figure 6, was analyzed. The overall displacement of the sample increased rapidly under all levels of load, which indicated that the elastic strain of the anchor was greater than the creep strain in the process of load increase. In a corrosive environment, the elastic strain produced by the load has an extremely important impact on the deformation of the anchored rock mass.

By analyzing Figure 6, it can be seen that the overall displacement of the sample is large, and the sample fails at an earlier time. Sample 10# will fail after the fifth-level load reaches the specified value.

With an increase in the load level, the overall deformation of specimens 2# and 10# increased, and the elastic deformation and creep deformation increased. With an increase in the number of corrosion days, the deformation of the sample also exhibited an increasing trend. When the corrosion time of the sample reached a certain value, the damage degree of the sample was too large, and the sample was damaged. With the increase in corrosion time, the load of the failure stage of the sample increased.

Figure 7 shows the surface crack characteristics of posttest failure.

3.2. Digital Image Analysis. It can be seen from Figure 8 that the strain in the middle of the sample is the largest at the initial stage of the test loading, and the strain in the middle of the sample also increases with an increase in the load and the passage of the test time. Combined with the diagram of the sample after loading in Figure 7(a), it can be observed that there are through cracks in the middle of the sample.

Figure 9 indicates that the strain in the upper part of the sample is greater than that in the lower part of the sample. During the test process, the strain on the surface of the sample increased continuously, and there were several obvious points in the middle of the sample where the strain

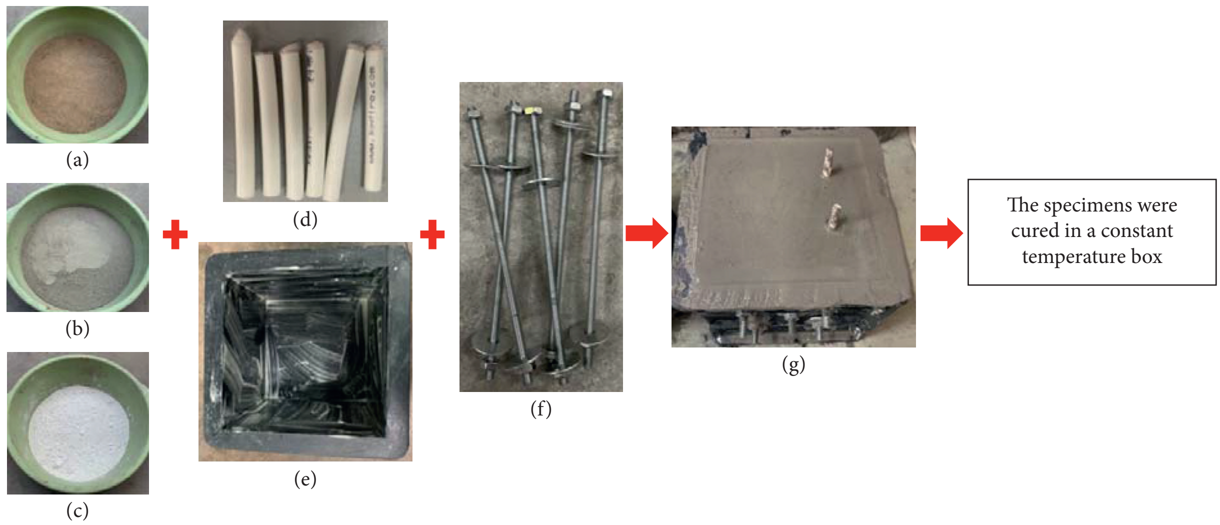

Figure 2: Fabrication process of the specimen. (a) River sand; (b) cement; (c) gypsum powder; (d) acid solution catheter; (e) mold coated with release agent; (f) bolt, gasket, and nut; (g) specimen after fabrication.

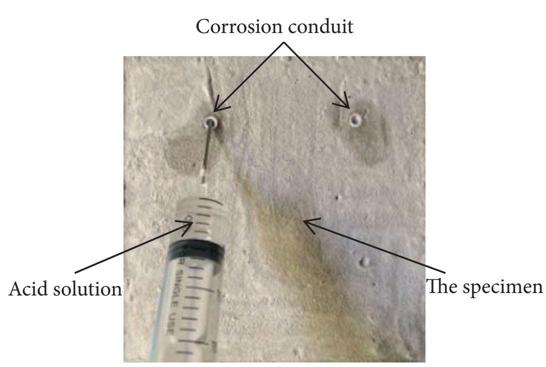

Figure 3: Schematic diagram of acid solution corrosion specimen.

Table 1: Parameters of test specimens.

Specimen	Number of corroded bolts	Number of noncorroded bolts	Diameter of anchor rod (mm)	Corrosion time (day)	Corrosion solution concentration (%)
2#	1	4	5	3	50
10#	1	4	5	14	50

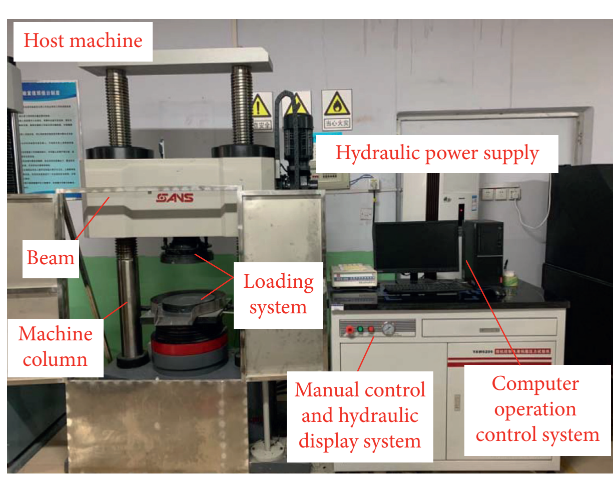

Figure 4: Universal pressure testing machine.

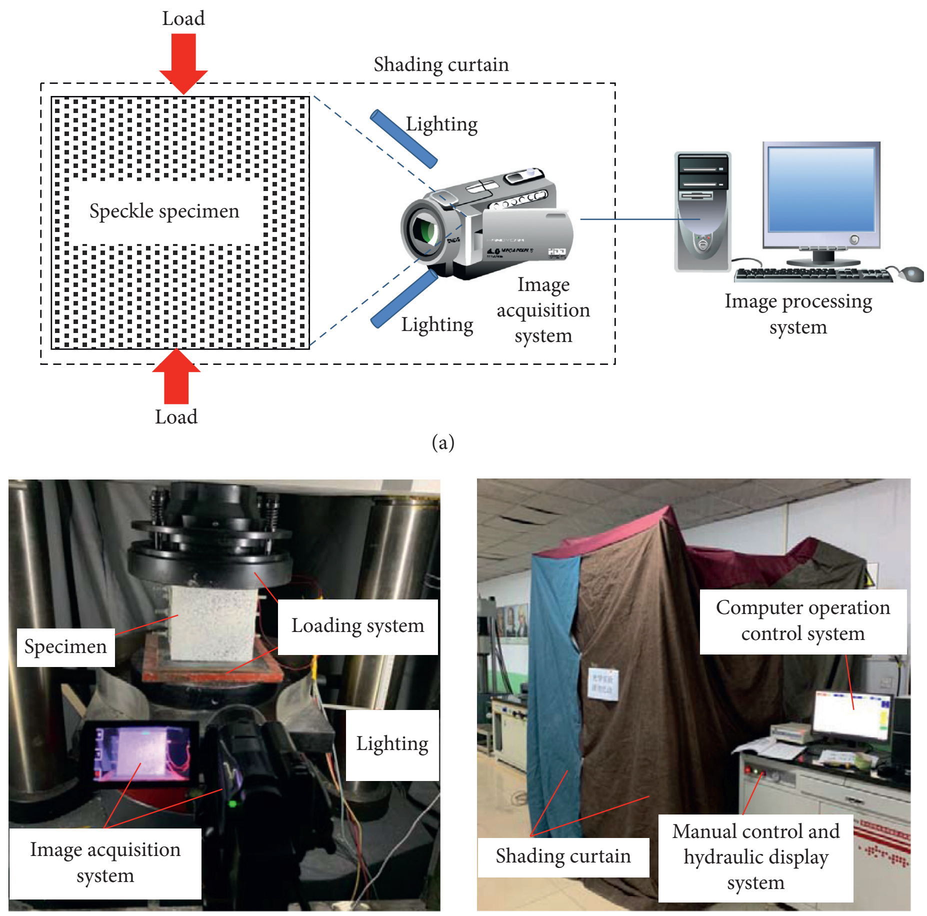

Figure 5: (a) Schematic diagram of digital speckle testing technology; (b) loading process diagram of specimen; (c) schematic diagram of shading treatment.

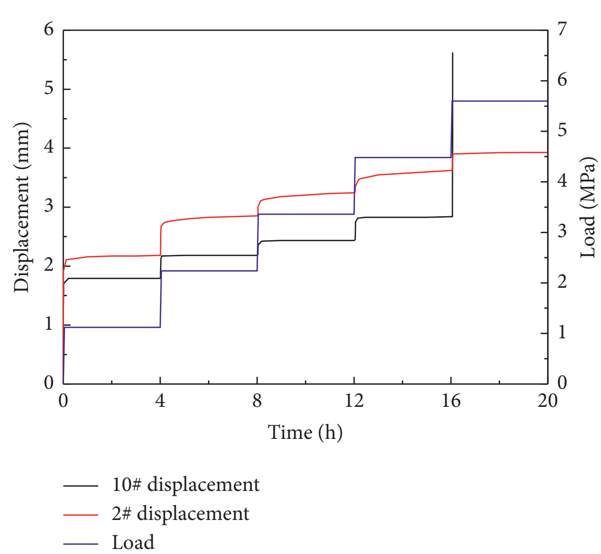

Figure 6: Loading path and overall deformation of specimens.

changed significantly, which was due to the cracks in the loading process of the sample.

Furthermore, in conjunction with Figure 6, it can be observed that the strain of the sample changes the most after the second stage load reaches the specified value, and cracks appear in the early loading process of the sample. The obvious strip cloud chart is perpendicular to the X-direction, indicating that the failure mode of the sample presents the

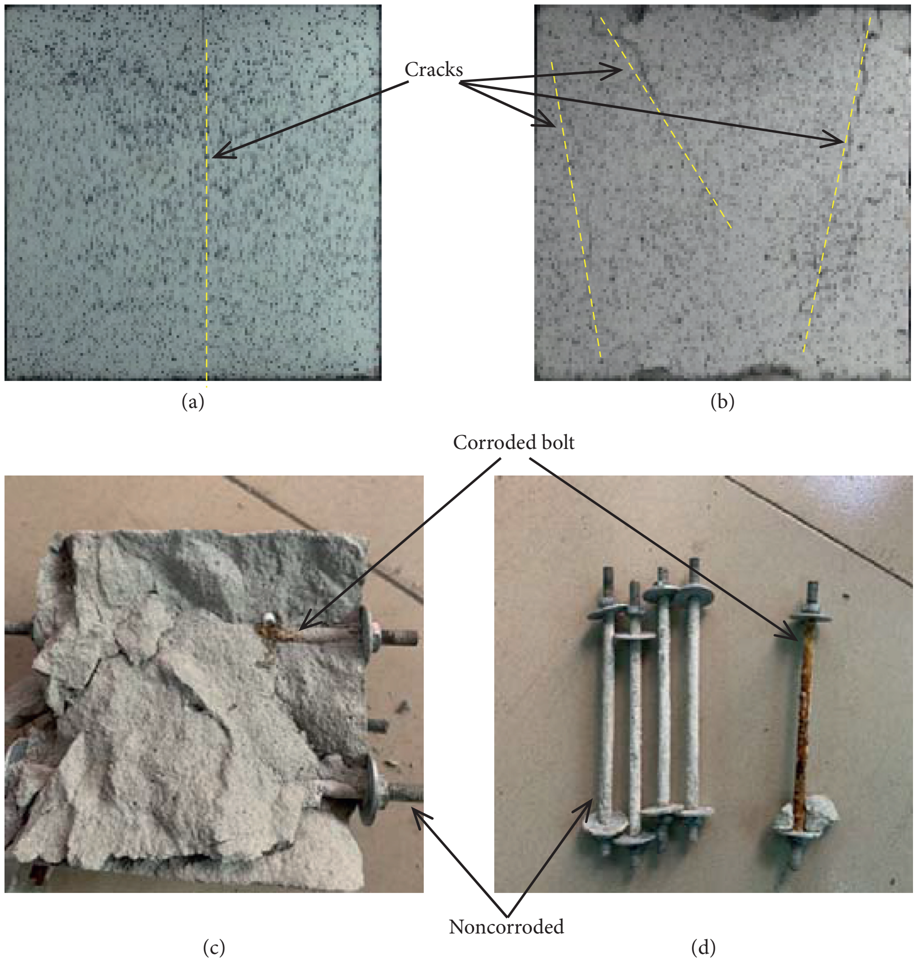

Figure 7: (a) Crack of specimen 2#; (b) cracks of specimen 10#; (c) comparison diagram of bolt in specimen; (d) comparison of corroded anchor and noncorroded anchor.

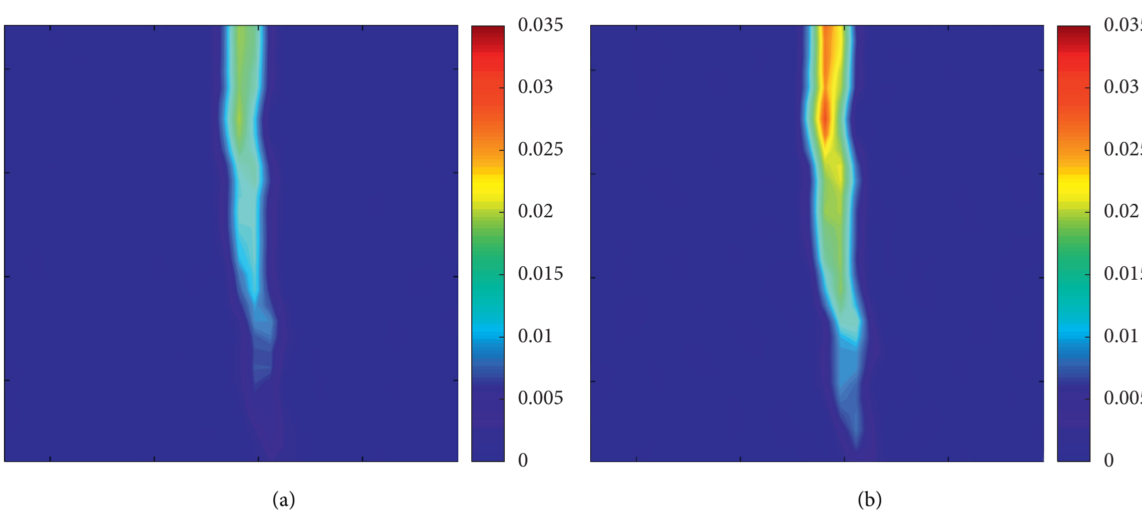

Figure 8: Continued.

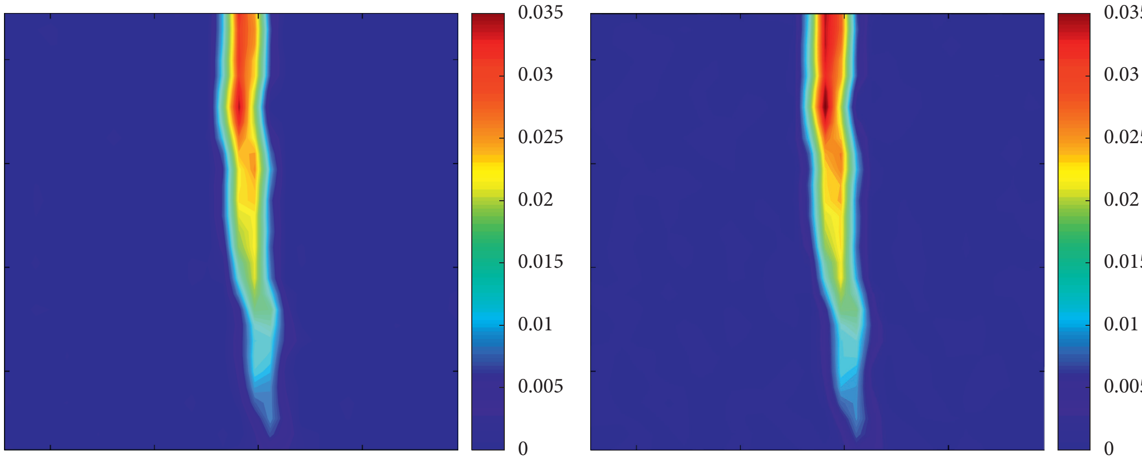

(c) (d)

Figure 8: X-direction strain nephogram of specimen 2# at different time: (a) 4 h; (b) 8 h; (c) 12 h; (d) 16 h.

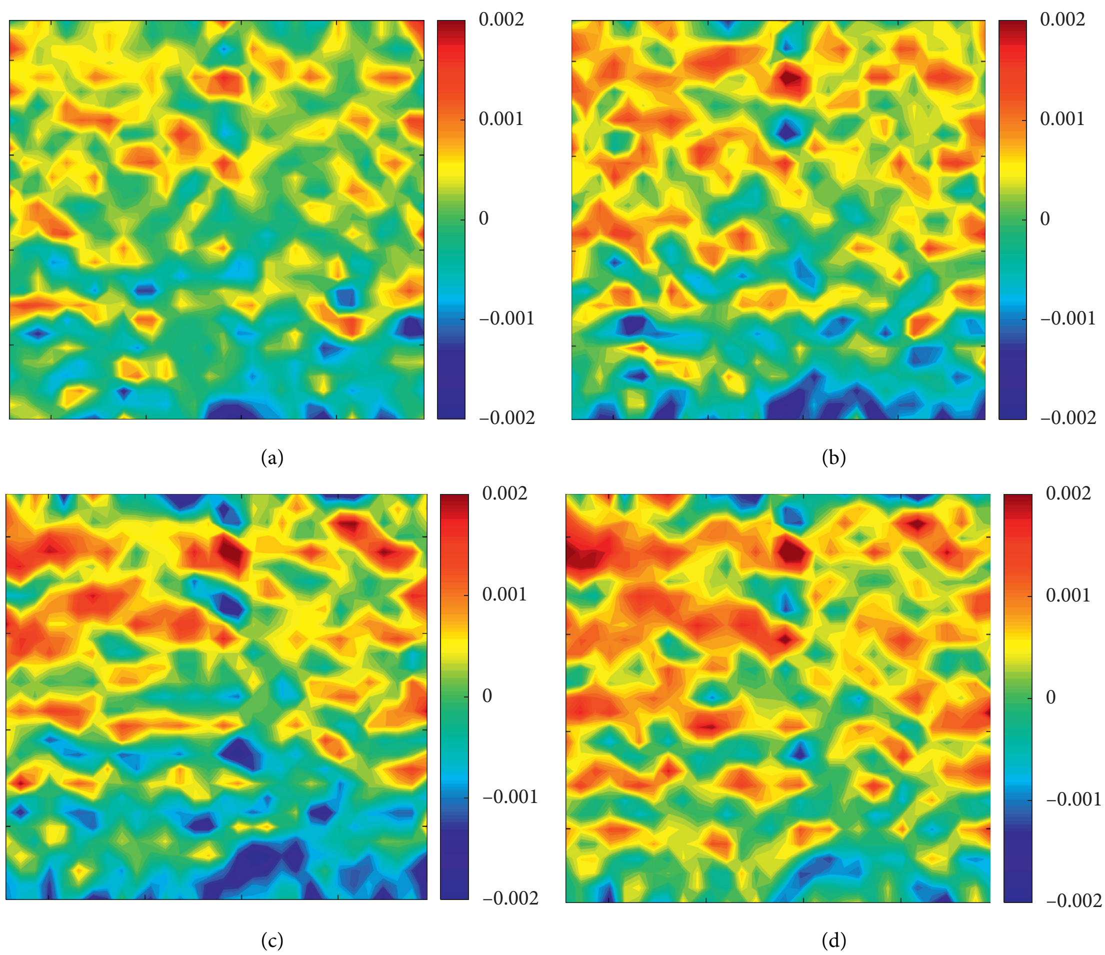

Figure 9: Y-direction strain nephogram of specimen 2# at different time: (a) 4 h; (b) 8 h; (c) 12 h; (d) 16 h.

splitting failure mode, which is consistent with the crack propagation law generated in the test process.

It can be observed from Figure 10 that the lower right part of the strain in the X-direction of sample 10# is larger than that of the upper left part at the initial stage of loading. When the third stage of loading was completed, the strain of the sample diffused from the lower right to the upper right. After the fourth stage, there were three positions with large strain

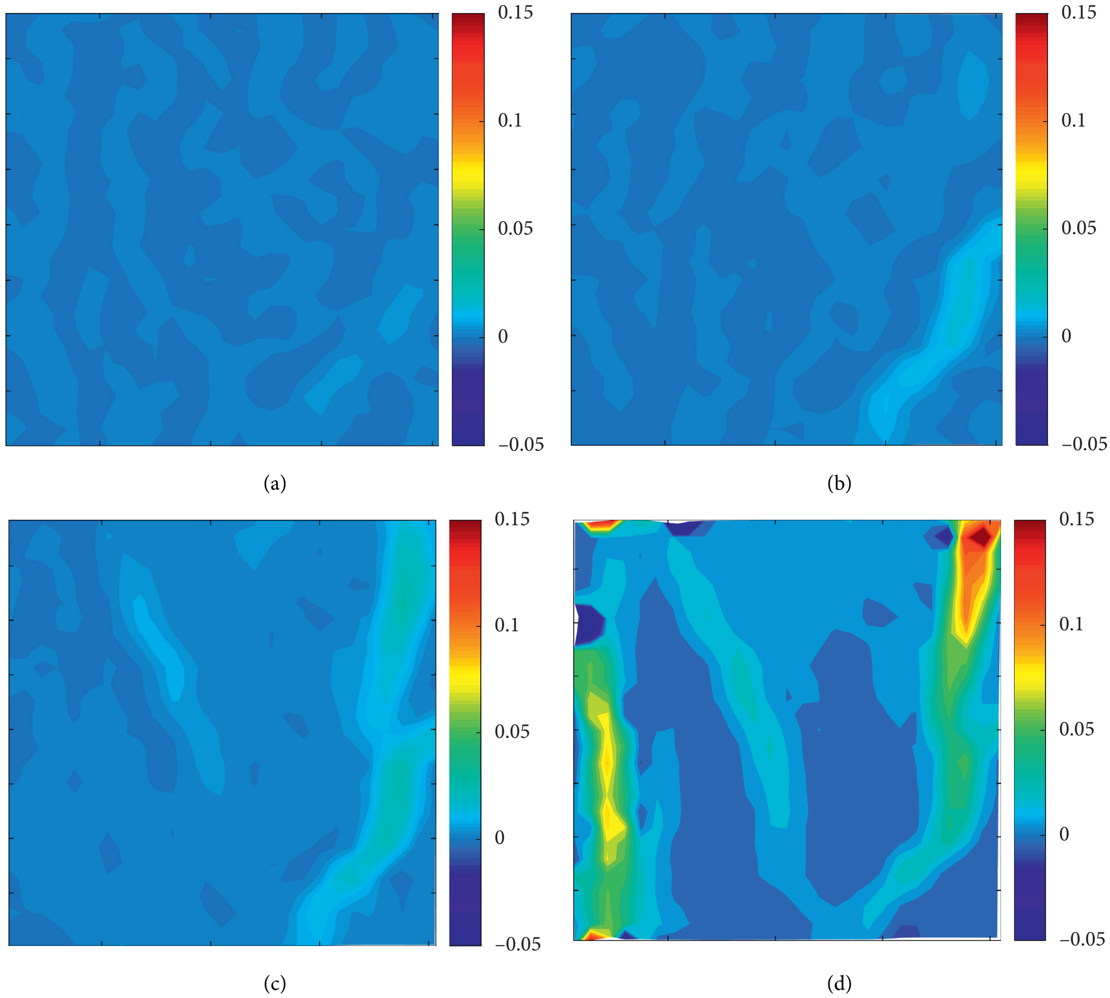

Figure 10: X-direction strain nephogram of specimen 10# at different time: (a) 4 h; (b) 8 h; (c) 12 h; (d) 16 h.

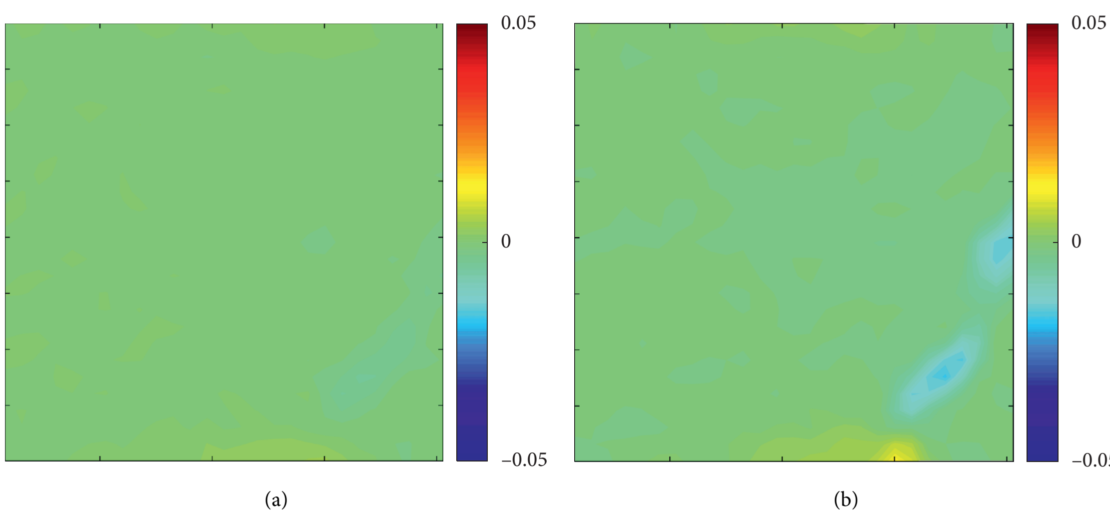

Figure 11: Continued.

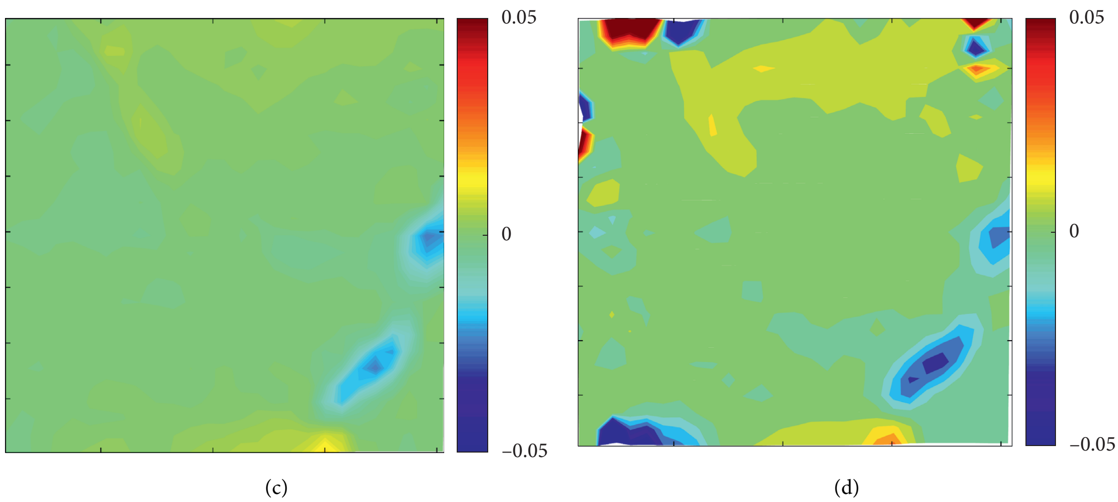

Figure 11: Y-direction strain nephogram of specimen 10# at different time: (a) 4 h; (b) 8 h; (c) 12 h; (d) 16 h.

changes on the surface of the sample, which further indicates that the location of failure cracks of the sample should be these three positions.

It can be observed from Figures 6 and 11 that the overall strain change in the Y-direction of sample 10# under the first three-stage loading is larger than that in the lower right part. During the four-stage loading process, the strain in the upper part of the sample begins to increase, and the strain change in the lower right part of the sample extends to the entire surface of the sample.

By combining Figures 6 and 11, it can be seen that the overall strain of sample 10# is mainly at the lower right during the first three stages of loading. With the passage of time and the improvement of the stage load level, the sample extends to three places where the strain changes significantly. This trend is consistent with the crack expansion and sample failure during the actual test process.

4. Conclusions

In this study, the influence of the corrosion environment on the creep characteristics of an anchor was systematically studied:

(i) With an increase in the level of loading, the overall deformation of the sample exhibited an increasing trend, in which the elastic deformation and creep deformation increased. With an increase in the corrosion time, the deformation of the sample also increased. When the corrosion time reached a certain value, the damage degree of the sample was too large, and the sample was damaged. With an increase in the corrosion time, the load of the failure stage of the sample increased. After the loading test, from the appearance of the two groups of specimens, it was found that the number of cracks on the surface of the 10# anchorage specimens was greater than that on the surface of specimens 2#.

(ii) During the test loading process, the strain of the specimen increased, and the load level increased. With the increase in corrosion time, the damage of the specimen becomes increasingly serious, and the mechanical properties of the specimen degenerate. The degree of damage of the specimen changed from the increasing strain of the specimen surface to the failure load of the specimen. Simultaneously, a significant corrosion layer appeared on the surface of the corroded bolt.

(iii) Under a corrosion environment, the strain in the lower part of the specimen is generally greater than that in the upper part of the specimen, and the failure of this group of specimens in the loading process is mostly splitting failure, which is basically generated along the trend of the strain nephogram, and shear failure occurs with the extension and diffusion of cracks. The abnormal area of the digital stress nephogram in the X-direction of the two groups of specimens is consistent with the crack height on the surface of the specimens.

Data Availability

The data are included in the article.

Conflicts of Interest

The authors declare no conflicts of interest.

Authors' Contributions

J. H. and H. W. designed the research methods. P. L. tested the specimens. G. S. analyzed the data and wrote the manuscript.

Acknowledgments

The research work has been greatly supported by Zhongyuan University of Technology and its staff in terms of test instruments and test methods. The funding for this investigation was provided by the National Natural Science

Foundation of China (no. 51574296), China Scholarship Council (no. 202008410379), and the Young Backbone Teachers of Zhongyuan University of Technology (no. 2018XQG14). The authors gratefully acknowledge the relevant organizations.

References

[1] S. Wu, H. Chen, H. Lamei Ramandi et al., "Investigation of cable bolts for stress corrosion cracking failure," *Construction and Building Materials*, vol. 187, pp. 1224–1231, 2018.

[2] S. Huang, X. Meng, G. Zhao et al., "Research and performance test of new full-length anchorage material," *Advances in Materials Science and Engineering*, vol. 2021, Article ID 9937751, 11 pages, 2021.

[3] J. Tian and L. Hu, "Review on the anchoring mechanism and application research of compression-type anchor," *Engineering*, vol. 8, no. 11, pp. 777–788, 2016.

[4] W. Ding, M. Li, M. Wang, R. Chen, Y. Wang, and L. Chen, "Experimental study on corrosion of anchored rock mass for half-through intermittent joints," *Advances in Civil Engineering*, vol. 2019, Article ID 6018678, 12 pages, 2019.

[5] W. Ding, M. Hou, L. Chen et al., "Experimental study on the deterioration rules of anchoring performance of rock mass under different joints distribution," *Advances in Civil Engineering*, vol. 2019, Article ID 3546052, 12 pages, 2019.

[6] M. W. T. Mak, P. Desnerck, and J. M. Lees, "Corrosion-induced cracking and bond strength in reinforced concrete," *Construction and Building Materials*, vol. 208, pp. 228–241, 2019.

[7] J. Dong, Y. Zhao, K. Wang, and W. Jin, "Crack propagation and flexural behaviour of RC beams under simultaneous sustained loading and steel corrosion," *Construction and Building Materials*, vol. 151, pp. 208–219, 2017.

[8] Y. Du, M. Cullen, and C. Li, "Structural performance of RC beams under simultaneous loading and reinforcement corrosion," *Construction and Building Materials*, vol. 38, pp. 472–481, 2013.

[9] M. Tahershamsi, I. Fernandez, K. Zandi, and K. Lundgren, "Four levels to assess anchorage capacity of corroded reinforcement in concrete," *Engineering Structures*, vol. 147, pp. 434–447, 2017.

[10] K. J. Ma, J. Stankus, and D. Faulkner, "Development and evaluation of corrosion resistant coating for expandable rock bolt against highly corrosive ground conditions," *International Journal of Mining Science and Technology*, vol. 28, no. 1, pp. 145–151, 2018.

[11] A. James, E. Bazarchi, A. A. Chiniforush et al., "Rebar corrosion detection, protection, and rehabilitation of reinforced concrete structures in coastal environments: a review," *Construction and Building Materials*, vol. 224, pp. 1026–1039, 2019.

[12] X. Zhang, L. Wang, J. Zhang, Y. Ma, and Y. Liu, "Flexural behavior of bonded post-tensioned concrete beams under strand corrosion," *Nuclear Engineering and Design*, vol. 313, pp. 414–424, 2017.

[13] Y.-C. Ou and N. D. Nguyen, "Influences of location of reinforcement corrosion on seismic performance of corroded reinforced concrete beams," *Engineering Structures*, vol. 126, pp. 210–223, 2016.

[14] M. M. Karthik, J. B. Mander, and S. Hurlebaus, "Simulating behaviour of large reinforced concrete beam-column joints subject to ASR/DEF deterioration and influence of corrosion," *Engineering Structures*, vol. 222, Article ID 111064, 2020.

[15] Y. Wang, X. Sun, and A. Ren, "Investigations of rock anchor corrosion and its influence factors by exhumations in four typical field sites," *Engineering Failure Analysis*, vol. 101, pp. 357–382, 2019.

[16] H. Lin, P. Sun, Y. Chen, Y. Zhu, X. Fan, and Y. Zhao, "Analytical and experimental analysis of the shear strength of bolted saw-tooth joints," *European Journal of Environmental and Civil Engineering*, vol. 2020, Article ID 1726822, 15 pages, 2020.

[17] H. Lin, Y. Zhu, J. Yang, and Z. Wen, "Anchor stress and deformation of the bolted joint under shearing," *Advances in Civil Engineering*, vol. 2020, pp. 1–10, 2020.

[18] J. Niu, W. Xu, J. Li, and J. Liang, "Influence of cross-sectional shape on the mechanical properties of concrete canvas and cfrp-reinforced columns," *Advances in Materials Science and Engineering*, vol. 2021, Article ID 5541587, 14 pages, 2021.

[19] A. Al-Sibahy and M. Sabhan, "Corrosion effects on the bond behaviour of steel bars in self-compacting concrete," *Construction and Building Materials*, vol. 250, Article ID 118568, 2020.

[20] Y. Zhang, E. Bicici, H. Sezen, and S. Zheng, "Reinforcement slip model considering corrosion effects," *Construction and Building Materials*, vol. 235, Article ID 117348, 2020.

[21] V. Marcos-Meson, G. Fischer, A. Solgaard, C. Edvardsen, and A. Michel, "Mechanical performance and corrosion damage of steel fibre reinforced concrete – a multiscale modelling approach," *Construction and Building Materials*, vol. 234, Article ID 117847, 2020.

[22] M.-C. Chen, C. Yang, W. Fang, and L. Xie, "A full-range analysis of anchorage failure for reinforced concrete beams in chloride environment," *Engineering Failure Analysis*, vol. 105, pp. 566–583, 2019.

[23] S. Imperatore, Z. Rinaldi, and S. Spagnuolo, "Influence of corrosion on the experimental behaviour of R.C. ties," *Engineering Structures*, vol. 198, Article ID 109458, 2019.

[24] A. O. Abdelatif, J. Ožbolt, and S. Gambarelli, "3D finite element modelling of corrosion of lap splice joints in concrete," *Construction and Building Materials*, vol. 169, pp. 124–131, 2018.

[25] Y. Ma, Z. Guo, L. Wang, and J. Zhang, "Experimental investigation of corrosion effect on bond behavior between reinforcing bar and concrete," *Construction and Building Materials*, vol. 152, pp. 240–249, 2017.

[26] D. W. Law and T. C. K. Molyneaux, "Impact of corrosion on bond in uncracked concrete with confined and unconfined rebar," *Construction and Building Materials*, vol. 155, pp. 550–559, 2017.

[27] C. G. Berrocal, I. Fernandez, K. Lundgren, and I. Löfgren, "Corrosion-induced cracking and bond behaviour of corroded reinforcement bars in SFRC," *Composites Part B: Engineering*, vol. 113, pp. 123–137, 2017.

[28] H. Lin, Y. Zhao, J. Ožbolt, and H.-W. Reinhardt, "Bond strength evaluation of corroded steel bars via the surface crack width induced by reinforcement corrosion," *Engineering Structures*, vol. 152, pp. 506–522, 2017.

[29] G. M. Hassan, "Deformation measurement in the presence of discontinuities with digital image correlation: a review," *Optics and Lasers in Engineering*, vol. 137, Article ID 106394, 2021.

[30] M. Moazzami, M. R. Ayatollahi, and A. Akhavan-Safar, "Assessment of the fracture process zone in rocks using digital image correlation technique: the role of mode-mixity, size, geometry and material," *International Journal of Damage Mechanics*, vol. 29, no. 4, 2020.

[31] A. Abdulqader and D. C. Rizos, "Advantages of using digital image correlation techniques in uniaxial compression tests," *Results in Engineering*, vol. 6, Article ID 100109, 2020.

[32] T. Wu, Y. Gao, Y. Zhou, and J. Li, "Experimental and numerical study on the interaction between holes and fissures in rock-like materials under uniaxial compression," *Theoretical and Applied Fracture Mechanics*, vol. 106, Article ID 102488, 2020.

[33] J. Tang, X. Chen, F. Dai, and M. Wei, "Experimental investigation of fracture damage of notched granite beams under cyclic loading using DIC and AE techniques," *Fatigue and Fracture of Engineering Materials and Structures*, vol. 43, no. 7, pp. 1583–1596, 2020.

[34] Y. Wang, L. Wang, F. Meng, and K. Chen, "Strength test of 3D printed artificial rock mass with pre-existing fracture," *Underground Space*, 2020.

[35] W. Dong, Z. Wu, X. Zhou, N. Wang, and G. Kastiukas, "An experimental study on crack propagation at rock-concrete interface using digital image correlation technique," *Engineering Fracture Mechanics*, vol. 171, pp. 50–63, 2017.

[36] J. Mata-Falcón, S. Haefliger, M. Lee, T. Galkovski, and N. Gehri, "Combined application of distributed fibre optical and digital image correlation measurements to structural concrete experiments," *Engineering Structures*, vol. 225, Article ID 111309, 2020.

[37] M. Sharafisafa, Z. Aliabadian, and L. Shen, "Crack initiation and failure of block-in-matrix rocks under Brazilian test using digital image correlation," *Theoretical and Applied Fracture Mechanics*, vol. 109, Article ID 102743, 2020.

[38] B. Tinkler-Davies and D. U. Shah, "Digital image correlation analysis of laminated bamboo under transverse compression," *Materials Letters*, vol. 283, Article ID 128883, 2021.

[39] F. Huang, C. Wu, P. Ni et al., "Experimental analysis of progressive failure behavior of rock tunnel with a fault zone using non-contact DIC technique," *International Journal of Rock Mechanics and Mining Sciences*, vol. 132, Article ID 104355, 2020.

[40] H. Zhang, G. Huang, H. Song, and Y. Kang, "Experimental investigation of deformation and failure mechanisms in rock under indentation by digital image correlation," *Engineering Fracture Mechanics*, vol. 96, pp. 667–675, 2012.

[41] S. Zhang, H. Wang, X. Li, X. Zhang, D. An, and B. Yu, "Experimental study on development characteristics and size effect of rock fracture process zone," *Engineering Fracture Mechanics*, vol. 241, Article ID 107377, 2020.

[42] C. M. Stewart and E. Garcia, "Fatigue crack growth of a hot mix asphalt using digital image correlation," *International Journal of Fatigue*, vol. 120, pp. 254–266, 2019.

[43] W. Liu, Y. Yu, Z. Zhang, C. Liu, and Y. Tong, "Impact resistance of CFRP-reinforced wood beams under axial force using a digital image correlation method," *Composite Structures*, vol. 261, Article ID 113276, 2020.

[44] R. Cao, H. Lin, and P. Cao, "Strength and failure characteristics of brittle jointed rock-like specimens under uniaxial compression: digital speckle technology and a particle mechanics approach," *International Journal of Mining Science and Technology*, vol. 28, no. 4, pp. 669–677, 2018.

[45] Z. Liang, J. Zhang, L. Qiu, G. Lin, and F. Yin, "Studies on deformation measurement with non-fixed camera using digital image correlation method," *Measurement*, vol. 167, Article ID 108139, 2021.

[46] X. P. Zhou, Y. J. Lian, L. N. Y. Wong, and F. Berto, "Understanding the fracture behavior of brittle and ductile multi-flawed rocks by uniaxial loading by digital image correlation," *Engineering Fracture Mechanics*, vol. 199, pp. 438–460, 2018.